Journal of Advanced Ceramics
2014, 3(1): 1–6
DOI: 10.1007/s40145-014-0087-z

ISSN 2226-4108
CN 10-1154/TQ

Research Article

Impedance spectroscopy study of $Na_2SmV_5O_{15}$ ceramics

P. S. DAS[a], P. K. CHAKRABORTY[a], Banarji BEHERA[b], N. K. MOHANTY[b], R. N. P. CHOUDHARY[c,*]

[a]*Department of Physics*, *Midnapore College*, *Midnapore 721 101*, *India*
[b]*School of Physics*, *Sambalpur University*, *Burla 768 019*, *Sambalpur*, *Odisha, India*
[c]*Department of Physics*, *ITER*, *Siksha "O" Anusandhan University*, *Bhubaneswar 751 030*, *Odisha*, *India*

Received: July 31, 2013; Revised: October 31, 2013; Accepted: November 10, 2013

Abstract: The polycrystalline $Na_2SmV_5O_{15}$ (NSV), a new member of the tungsten bronze (TB) family, was prepared by a mixed-oxide technique. The room-temperature X-ray diffraction (XRD) confirmed the formation of single phase compound with orthorhombic crystal structure. The scanning electron microscopy (SEM) analysis indicated that the compound has homogeneous micrograph with a uniform distribution of small grains over the entire surface of the sample. The analysis of impedance spectra of NSV in a low-temperature range (−100 ℃ to 100 ℃) at different frequencies exhibited interesting electrical properties like the contribution of bulk effect in conduction process. The study of imaginary part of the impedance at different temperatures showed existence of relaxation peak with its shift towards higher frequency on increasing temperature. This suggested the presence of frequency and temperature dependent relaxation process in the material. The loss peak spectra were found to abide by Arrhenius law with small activation energy of 0.12 eV. The temperature dependence of AC and DC electrical conductivity (σ_{AC} and σ_{DC}) was also obtained.

Keywords: solid-state reaction; microstructure; impedance; conductivity

1 Introduction

Due to the structural versatility of vanadium-containing compounds, some vanadates have attracted much attention of the researchers to work in such new compounds. They also have the ability to act as intercalation, ion-exchange, magnetism, cathode, and nonlinear optical (NLO) materials [1–7]. In vanadates, vanadium has been found in three-, four-, five-, and six-coordinate environments. Generally, the known ferroelectric oxides have perovskite, tungsten bronze (TB) or pyrochlore structures. Nowadays, there has been much interest to study the TB ferroelectric vanadates because they have useful applications. The TB structure with a general formula $(A_1)_2(A_2)_4(C)_4$-$(B_1)_2(B_2)_8O_{30}$ is a network of octahedral sharing of corners of a unit cell, and hence it would be easily said that this structural family stands at an intermediate position of perovskite and pyrochlore types of structures. A TB unit cell is composed of ten octahedral and six cages; the cage consists of four 15-coordinated sites and two 12-coordinated sites, surrounded by the octahedral. The octahedral sites are occupied by B ions and the remaining six sites by A ions, and the compound is generally represented by the formula

* Corresponding author.
E-mail: crnpfl@gmail.com

$A_6B_{10}O_{30}$ (called a filled TB), where either A or B sites are to be occupied by more than two kinds of ions. Accordingly, if the binary system is composed of A and B oxides, we could only find one $A_5B_{10}O_{30}$ TB type where six A sites are occupied by five ions; this is a typical TB structure. Though a lot of work on the niobates and vanadates of TB structural family have been reported in the past [8–14], we could not find any work on the titled compound. Giess *et al*. [13] reported the structural and dielectric properties of $KPb_2Nb_5O_{15}$ with Pb and K at the A site and Nb at the B site of TB structure. In view of the importance of materials within this family, we have attempted to study the synthesis, structure and electrical properties (impedance parameters) of $Na_2SmV_5O_{15}$ (NSV) ceramics by the substitutions of Na at the A site and V at the B site of the TB structure.

2 Experiment

Using a mixed-oxide method, the polycrystalline sample of NSV was prepared relatively at low temperature (450 ℃), with high-purity (>99%) ingredients: Na_2CO_3 (M/s. Sarabhai Chemicals, India), Sm_2O_3 (M/s. Loba Chem. Ltd, India) and V_2O_5 (M/s. Koch Light Ltd, England). The ingredients were thoroughly mixed in air atmosphere for 1 h and then in methanol atmosphere for 1 h. The mixed powder was calcined for 7 h at an optimum temperature (450 ℃) in an alumina crucible. The X-ray diffraction (XRD) analysis confirmed the formation of a new compound. The calcined powder was then cold-pressed into cylindrical pellets at a pressure of 4×10^6 N/m^2 using a hydraulic press. As a binder, polyvinyl alcohol was used to prepare pellets, and burnt out during the high-temperature sintering. The sample was sintered at the temperature of 475 ℃ (optimized) in an alumina crucible in air atmosphere for 7 h. The pellets were polished by fine emery papers to make the surfaces flat and parallel. The flat surfaces were coated with silver paint. After electroding, the pellets were dried at a temperature of 150 ℃ for 4 h to remove moisture and then brought to room temperature before taking electrical measurements. Structural data were recorded by X-ray diffractometer (Rigaku Miniflex, Japan) using Cu Kα radiation ($\lambda=1.5405$ Å) in a wide range of Bragg angle 2θ ($20°\leqslant2\theta\leqslant80°$) with a scanning rate of 4 (°)/min. The electrical properties were measured by a computer-controlled LCR meter (HIOKI Model: 3532) in a wide range of frequency (10^2–10^6 Hz) at different temperatures (−100 ℃ to 100 ℃).

3 Results and discussion

3.1 Structural and micro structural properties

The room-temperature XRD pattern of the calcined powder of NSV is shown in Fig. 1. It shows the formation of a new single-phase compound. All of the reflection peaks are indexed in different crystal systems and unit cell configuration. An orthorhombic unit cell is selected on the basis of the good agreement between observed and calculated d spacing ($\sum\Delta d=d_{\text{obs}}-d_{\text{cal}}=$ minimun). The lattice parameters of the selected unit cell were refined using the least-squares sub-routine of a standard computer program package "POWD" [15]. These are $a=18.0487(33)$ Å, $b=16.9000(33)$ Å, $c=3.4986(33)$ Å, and $V=1067.14$ Å^3 (the number in parenthesis is estimated standard deviation). These unit cell parameters are in good agreement with those of reported ones [14,15] for the TB structure. However, with limited data, it is not possible to determine crystal structure and the space group of the compound. The average crystallite size (P) of NSV is determined from the broadening of a few XRD peaks using the Scherrer's equation [16]:

$$P=K\lambda/(\beta_{1/2}\cos\theta_{hkl})$$

where $K=0.89$ (constant); $\lambda=1.5405$ Å; $\beta_{1/2}$ is the peak width of the reflection at half intensity; and

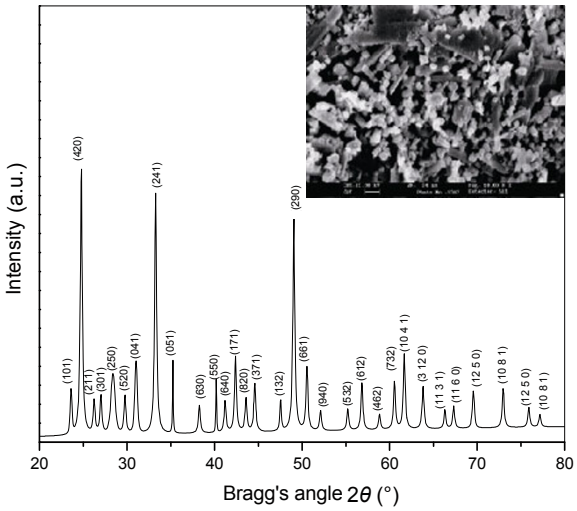

Fig. 1 Room-temperature XRD and SEM (inset) patterns of NSV.

θ_{hkl} is the Bragg angle. The average crystallite size of the compound is found to be 47 nm. The scanning electron microscopy (SEM) obtained using a scanning electron microscope (Model LEICA S440i) of the sample is given in Fig. 1 (inset), which clearly shows uniform distribution of the grains over the entire surface with certain degree of porosity.

3.2 Impedance analysis

Impedance spectroscopy is a powerful technique for the characterization of electrical behavior of electro-ceramic materials, where a sinusoidal perturbation is applied and the AC response is analyzed. Subsequently, impedance is calculated as a function of frequency of the perturbation. The output response appears in the form of a succession of semicircle representing electrical phenomena due to bulk, grain boundary effect and interfacial phenomena in the Argand plane [17]. Though polycrystalline materials usually show both grain and grain boundary effects with different time constants leading to two successive semicircles, in this present study, within the chosen temperature and frequency ranges, the second intercept corresponding to the low-frequency semicircle exhibiting grain boundary property is not observed. The frequency-dependent electrical properties of a material are represented in terms of complex impedance Z^*, as

$$Z^*(\omega)=Z'-\mathrm{j}Z''=R_\mathrm{s}-1/(\mathrm{j}\omega C_\mathrm{s})$$

where Z' and Z'' are the real and imaginary components of impedance, respectively; $\mathrm{j}=\sqrt{-1}$ is the imaginary factor; and R_s is the series resistance and C_s is the series capacitance.

The complex impedance plots of the material are obtained at different temperatures shown in Fig. 2. The presence of well-resolved semicircular arcs with rise in temperature has been attributed to the bulk properties of the material, and arises due to the parallel combination of bulk resistance R_b and bulk capacitance C_b. The low-frequency dispersion curve (second semicircular arc) not appearing in our selected temperature range can be assigned to the grain boundary. The intercept of the first semicircular arc on the real axis Z' gives the bulk resistance R_b (DC resistance). The DC resistance decreases on increasing temperature. This nature indicates that the bulk conductivity of the material increases with increase of temperature. Thus the material shows negative temperature coefficient of resistance (NTCR), which is a property of semiconductors. The grain and grain boundary effects can be modeled as cascading of parallel RC combination in accordance with brick layer model [18], which has been represented in terms of the equivalent circuit given in Fig. 2 (inset). The value of the circuit elements obviously depends microscopically on the volume fraction of the grain; such a substantial decrease in the value of R_b has been observed with rise in temperature. All these curves start at almost the same R_b value, and do not coincide with the origin. So there would be a series of resistance that can be ascribed to the LCR circuit representation of the sample. The peak maxima of the plot decreases and shifts towards higher values with rise in temperature. This curve helps to determine the particle interaction like grain and grain boundary effects etc. This provides the information about the nature of the dielectric relaxation. For pure non-dispersive Debye process, one expects semicircular plots with the centre located on the Z' axis. For the poly-dispersive relaxation, these Argand plane [17] plots are close to the circular arcs with end points on the real axis, and the centre below it as observed in the present study. The complex impedance in such situation is described by Cole formalism:

$$Z^*(\omega)=Z'+\mathrm{i}Z''=R/[1+(\mathrm{i}\omega/\omega_0)^{1-\alpha}]$$

where α is the magnitude of the departure of the electrical response from an ideal condition and this can be determined from the location of the centre of the circles (not shown here); ω_0 is the Debye frequency. When α tends to zero, we have classical Debye

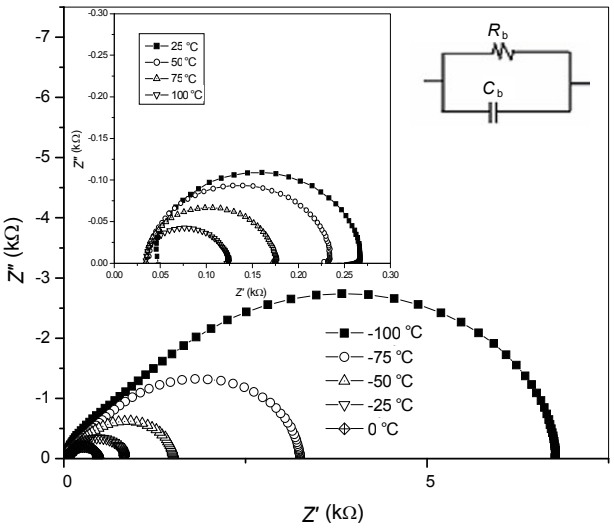

Fig. 2 Variation of Z'' and Z' at selected temperatures with equivalent circuit (inset).

formalism [19]. From these figures, it is clear that the dominance is only grain resistance. As the temperature increases, the bulk resistance which shows the NTCR behavior decreases like that of a semiconductor.

Figure 3 shows loss spectra (i.e., the variation of the imaginary part of the impedance Z'' with frequency) at different temperatures. This provides an insight into the process associated with the largest resistance. The loss spectra have a few important features: (i) typical peak broadening with rise in temperatures and (ii) asymmetric peak broadening. The presence of peak at unique frequency indicates the type and strength of electrical relaxation phenomenon in the material. The peak broadening with temperature indicates the temperature-dependent relaxation phenomenon in the material. At low temperatures, the relaxation phenomenon may be due to the immobile species/ electrons; at high temperatures, the relaxation may be due to the defects/vacancies. The decrease in the magnitude of Z'' with a shift in the peak frequency towards higher frequency arises possibly due to the presence of space charges at higher temperatures. The asymmetric broadening of the peaks suggests that multiple relaxation phenomenon is present in the material, with their own discrete relaxation time depending on the temperature. The relaxation peak in the loss spectrum coincides with the highly dispersive region in the Z' vs. frequency spectrum.

The variation of the real part of impedance Z' with frequency at several temperatures is shown in Fig. 4. It exhibits that Z' decreases with rise in frequency and temperature. The values of Z' merge after a certain frequency. This may be due to release of space charges

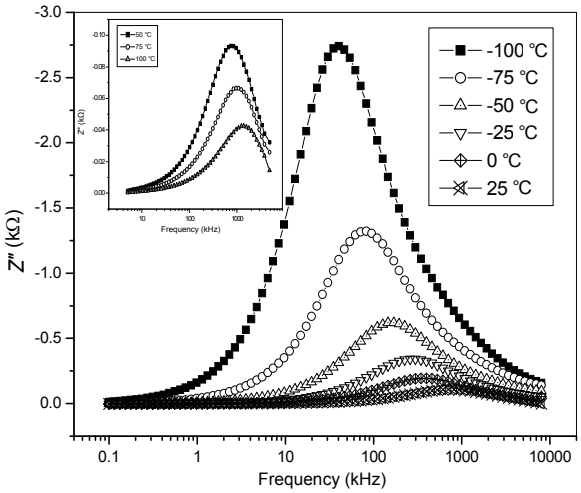

Fig. 3 Variation of Z'' with frequency at a few selected temperatures.

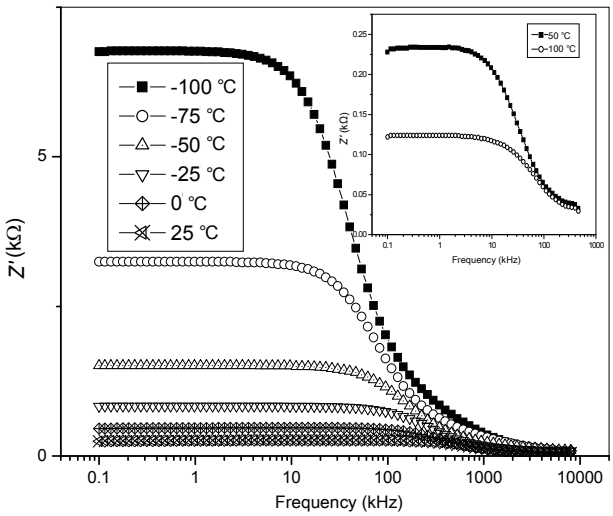

Fig. 4 Variation of Z' with frequency at a few selected temperatures.

at low temperatures. It indicates increment in AC conductivity with increment of temperature and frequency. As the temperature increases, the nature of variation of Z' as a function of frequency assumes a sigmoid type in the low-frequency region, and a plateau region beyond a fixed frequency. The magnitude of Z' (bulk resistance) decreases with increasing temperature, and appears to merge in the high-frequency region, irrespective of temperature. The behavior at high temperature may be attributed to the lowering of barrier properties of the sample with temperature, and then space charges would be emitted, which would enhance the conductivity and reduce the impedance properties. The modulus of Z' decreases with the rise in temperature, which means the sample exhibits NTCR behavior which is consistent with the previous results. This behavior is changed drastically in the high-frequency region. This particular frequency at which Z' value becomes constant is observed to shift towards the high-frequency side with rise of temperature. This shift in Z' plateau indicates the possibility of frequency relaxation process in the material.

4 Electrical conductivity

4.1 AC conductivity

The variation of AC conductivity (σ_{AC}) as a function of frequency (conductivity spectrum) at different temperatures is shown in Fig. 5. The conductivity

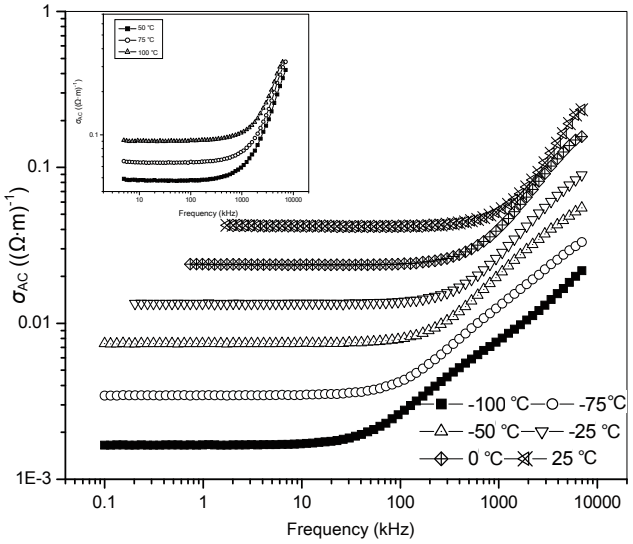

Fig. 5 Variation of σ_{AC} as a function of frequency at selected temperatures.

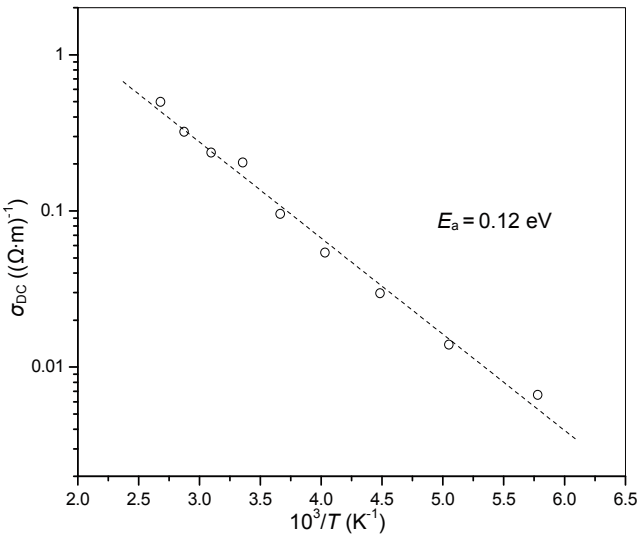

Fig. 6 Variation of σ_{DC} with $10^3/T$.

patterns can be divided into two parts. First at low temperatures, continuous dispersion curves of conductivity are observed in the lower-frequency region. Then the conductivity patterns approach close to each other in the high-frequency region for the same temperature region. This may be attributed to the space charge dependent region. The plateau region corresponds to the frequency-independent σ_{DC} conductivity. The rise in the conductivity value with temperature indicates that the electrical conduction is a thermally activated process.

4.2 DC conductivity

The typical variation of σ_{DC} with temperature is a characteristic that the conductivity increases with the increment of temperature (Fig. 6). This is a typical Arrhenius type behavior:

$$\sigma_{DC} = \sigma_0 \exp[-E_a / (kT)]$$

where σ_{DC} is the DC conductivity; σ_0 is the pre-exponential factor; E_a is the activation energy; and k is the Boltzmann constant. The activation energy calculated from the slope of straight line is found to be 0.12 eV. The value of activation energy is found to be very less as compared to other TB and perovskite structure compounds [20–22]. This suggests that a small amount of energy is required to activate the electrons for electrical conduction.

The impedance data are used to evaluate the relaxation time (τ) of the electrical process in the material using the relation:

$$\omega_{max}\tau = \omega_{max} R_b C_b = 1$$

where ω_{max} is the maximum angular frequency; R_b and C_b are the bulk resistance and bulk capacitance respectively. It is independent of the sample geometry factors, but depends only on its intrinsic property (microstructure). The pattern shows a steady decrease in magnitude with rise in temperature (Fig. 7). This suggests the occurrence of temperature-dependent electrical relaxation phenomenon. This may be due to the migration of immobile species/defects. It is found to obey the Arrhenius law:

$$\tau = \tau_0 \exp[-E_a / (kT)]$$

where τ is the relaxation time; τ_0 is the pre-exponential factor; E_a is the activation energy; and k is the Boltzmann constant. This expression

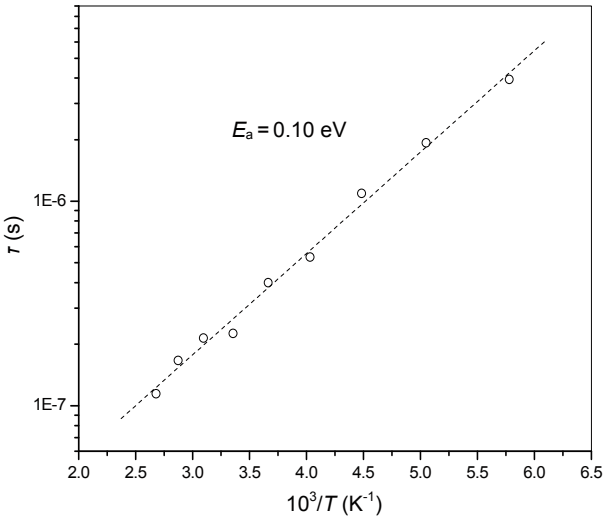

Fig. 7 Variation of relaxation time (τ) with $10^3/T$.

also estimates the activation energy which has a close resemblance to previously obtained E_a, and hence suggests the possibility of long-range mobility of charge carriers (ions) via hopping combination mechanism at higher temperatures.

5 Conclusions

The polycrystalline sample of NSV, a new member of TB structural family, was prepared by a mixed-oxide method at relatively low temperature (450 ℃). Preliminary X-ray analysis exhibited the orthorhombic crystal structure of the compound at room temperature. Impedance spectroscopy was used to characterize the electric properties of the material. The material showed the NTCR behavior which is the characteristics of a semiconductor. Study of the temperature dependence of DC conductivity provided activation energy with the value of 0.12 eV.

References

[1] Cavalli E, Belletti A, Mahiou R, *et al*. Luminescence properties of $Ba_2NaNb_5O_{15}$ crystals activated with Sm^{3+}, Eu^{3+}, Tb^{3+} or Dy^{3+} ions. *J Lumin* 2010, **130**: 733–736.

[2] Yin X, Shi L, Wei A, *et al*. Effect of structural packing on the luminescence properties in tungsten bronze compounds $M_2KNb_5O_{15}$ (M = Ca, Sr, Ba). *J Solid State Chem* 2012, **192**: 182–185.

[3] Szwagierczak D, Kulawik J. Thick film capacitors with relaxor dielectrics. *J Eur Ceram Soc* 2004, **24**: 1979–1985.

[4] Alaoui-Belghiti HE, Von der Mühll R, Simon A, *et al*. Relaxor or classical ferroelectric behavior in ceramics with composition $Sr_{2-x}A_{1+x}Nb_5O_{15-x}F_x$ (A = Na, K). *Mater Lett* 2002, **55**: 138–144.

[5] Ranga Raju MR, Choudhary RNP. Diffuse phase transition in $Sr_5RTi_3Nb_7O_{30}$ (R = La, Nd and Sm). *J Phys Chem Solids* 2003, **64**: 847–853.

[6] Rani R, Sharma S, Rai R, *et al*. Dielectric behavior and impedance analysis of lead-free CuO doped $(Na_{0.50}K_{0.50})_{0.95}(Li_{0.05}Sb_{0.05}Nb_{0.95})O_3$ ceramics. *Solid State Sci* 2013, **17**: 46–53.

[7] Ramam K, Chandramouli K. Ferroelectric and pyroelectric properties of Ce^{3+} modified tetragonal tungsten bronze structured lead barium niobate-55 ceramics. *J Phys Chem Solids* 2012, **73**: 1061–1065.

[8] Singh AK, Choudhary RNP. Diffuse ferroelectric phase transition in $Pb_5RTi_3Nb_7O_{30}$ (R = Eu and Gd). *Mater Lett* 2003, **57**: 3722–3728.

[9] Ravez J, Alaoui-Belghiti HE, Elaatmani M, *et al*. Relations between ionic order or disorder and classical or relaxor ferroelectric behaviour in two lead-free TKWB-type ceramics. *Mater Lett* 2001, **47**: 159–164.

[10] McCabe EE, West AR. New high permittivity tetragonal tungsten bronze dielectrics $Ba_2LaMNb_4O_{15}$: M = Mn, Fe. *J Solid State Chem* 2010, **183**: 624–630.

[11] Kathayat K, Panigrahi A, Pandey A, *et al*. Structural and electrical studies of $Ba_5RTi_3V_7O_{30}$ (R = Ho, Gd, La) compounds. *Physica B* 2012, **407**: 3753–3759.

[12] Parida BN, Das PR, Padhee R, *et al*. A new ferroelectric oxide $Li_2Pb_2Pr_2W_2Ti_4Nb_4O_{30}$: Synthesis and characterization. *J Phys Chem Solids* 2012, **73**: 713–719.

[13] Giess EA, Scott BA, Burns G, *et al*. Alkali strontium–barium–lead niobate systems with a tungsten bronze structure: Crystallographic properties and Curie points. *J Am Ceram Soc* 1969, **52**: 276–281.

[14] Mohanty NK, Satpathy SK, Behera B, *et al*. Complex impedance properties of $LiSr_2Nb_5O_{15}$ ceramic. *J Adv Ceram* 2012, **1**: 221–226.

[15] Wu E. *POWD*, an interactive program for powder diffraction data interpretation and indexing. *J Appl Cryst* 1989, **22**: 506–510.

[16] Patterson A. The Scherrer formula for X-ray particle size determination. *Phys Rev* 1939, **56**: 978–982.

[17] Shaw WT. *Complex Analysis with Mathematica*. Cambridge(UK): Cambridge University Press, 2006.

[18] Kidner NJ, Homrighaus ZJ, Ingram BJ, *et al*. Impedance/dielectric spectroscopy of electroceramics—Part 2: Grain shape effects and local properties of polycrystalline ceramics. *J Electroceram* 2005, **14**: 293–301.

[19] Hill RM, Dissado LA. Debye and non-Debye relaxation. *J Phys C*: *Solid State Phys* 1985, **18**: 3829–3836.

[20] Behera B, Nayak P, Choudhary RNP. Structural, dielectric and impedance properties of $NaCa_2V_5O_{15}$ ceramics. *Curr Appl Phys* 2009, **9**: 201–205.

[21] Behera B, Nayak P, Choudhary RNP. Impedance spectroscopy study of $NaBa_2V_5O_{15}$ ceramic. *J Alloys Compd* 2007, **436**: 226–232.

[22] Liu L, Huang Y, Su C, *et al*. Space-charge relaxation and electrical conduction in $K_{0.5}Na_{0.5}NbO_3$ at high temperatures. *Appl Phys A* 2011, **104**: 1047–1051.